Organic Process Research & Development

ARTICLE

pubs.acs.org/OPRD

Separation of Racemic Bicalutamide by an Optimized Combination of Continuous Chromatography and Selective Crystallization

Henning Kaemmerer,[*,†,‡,¶] Zoltan Horvath,[‡] Ju Weon Lee,[‡] Malte Kaspereit,[§,#] Robert Arnell,[⊥] Martin Hedberg,[⊥] Björn Herschend,[⊥] Matthew J. Jones,[⊥] Kerstin Larson,[⊥] Heike Lorenz,[‡] and Andreas Seidel-Morgensten[‡]

[†]Evonik Industries AG, 63457 Hanau, Germany

[‡]Physical and Chemical Foundations of Process Engineering, Max Planck Institute for Dynamics of Complex Technical Systems, 39106 Magdeburg, Germany

[§]Process Synthesis and Process Dynamics, Max Planck Institute for Dynamics of Complex Technical Systems, 39106 Magdeburg, Germany

[⊥]AstraZeneca R&D Södertälje, Pharmaceutical Development, 15185 Södertälje, Sweden

Supporting Information

ABSTRACT: A racemic mixture of bicalutamide, a drug substance used in the treatment of prostate cancer, was separated by simulated moving bed chromatography, with the objective of maximizing throughput at reduced outlet purity. The enriched extract stream was purified further by a crystallization process exploiting a shift in the eutectic composition. The optimal purity in between both process steps was identified. The separation scheme developed was validated on a scale of 600 g, and the results were compared to those of state-of-the art and discussed. The investigated scheme revealed a wide range of promising coupling conditions while showing superior productivities and enhanced process robustness.

1. INTRODUCTION

(*R*)-Bicalutamide (compound **1**, Figure 1) is the active pharmaceutical ingredient (API) in AstraZeneca's product CASODEX. The compound is an orally active, once-a-day nonsteroidal anti-androgen for the treatment of prostate cancer.[1] CASODEX is the racemate of bicalutamide. The manufacturing method designed during a development program within AstraZeneca for the purpose of manufacturing the pure (*R*)-enantiomer of bicalutamide (compound **2**, Figure 1), utilizes SMB-HPLC for full enantioseparation, followed by crystallization of pure, crystalline solid from methanol−water to obtain the required purity and solid-state properties of the API.

An analysis of the published asymmetric syntheses of both (*R*)- and (*S*)-bicalutamide leads to the conclusion that all available methods lack industrial potential for various reasons such as low overall yield or high cost of raw materials.[2−10] Consequently, the racemate, which is produced using an efficient and cost-effective chemical process (not shown), is currently the cheapest source of the pure enantiomer.

Furthermore, the overall efficiency of the manufacturing process for the active (*R*)-enantiomer could be further improved, providing a method for the efficient and economic conversion of the undesired (*S*)-enantiomer of bicalutamide were available. Since the internal AstraZeneca process design was developed to perform full enantioseparation of the racemic material, it should be possible to improve significantly the capacity of the chromatography process developed using process integration concepts developed within the European Union funded Framework Program 7-project INTENANT.[11]

Previous internal studies at AstraZeneca on the crystallization of the pure enantiomer of bicalutamide did not comprehensively investigate the temperature and solvent dependence of the position of the eutectic for this racemic compound forming system. As will be shown in this article, detailed characterization[24] of the crystallization behavior of bicalutamide, provides insight into new possibilities in terms of process solutions for manufacturing the desired (*R*)-enantiomer.

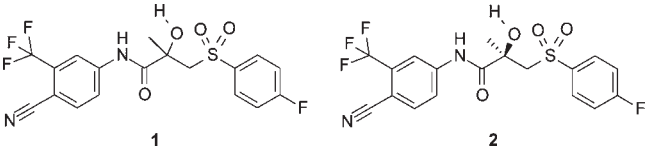

Figure 1. Structures of racemic bicalutamide 1 and the pure (*R*)-enantiomer 2.

2. DESIGN AND SETUP OF A CHROMATOGRAPHIC PRE-ENRICHMENT STEP

2.1. Experimental Section I: Parameter Determination for Chromatography. *2.1.1. Chromatographic System.* An initial screening procedure revealed good performance of the stationary phase Chiralpak AD (Daicel Chemical Industries Ltd.). Within this study, the adsorption behavior of the two enantiomers onto the stationary phase was investigated using an analytical column with dimensions of 250 mm ×

Special Issue: INTENANT

Received: May 26, 2011
Published: September 19, 2011

dx.doi.org/10.1021/op200136z | *Org. Process Res. Dev.* 2012, 16, 331–342

Table 1. Column efficiency measured for (*S*)-bicalutamide (1) and (*R*)-bicalutamide (2) as a function of flow rate

u_0					
mL/min	cm/min	NTP_1	NTP_2	$HETP_1$ mm	$HETP_2$ mm
1	6.02	432	288	0.58	0.87
2	12.03	499	213	0.50	1.17
3	18.05	432	126	0.58	1.98
3	18.05	417	122	0.60	2.05
4	24.07	390	88	0.64	2.84
5	30.09	336	89	0.74	2.81

4.6 mm packed with a preparative chiral stationary phase with a particle size of 20 μm. Pure methanol was used as mobile phase.

2.1.2. Axial Dispersion and Mass Transfer. Using the above column, the total porosity was determined as $\varepsilon_T = 0.622$ from an injection of a nonretained compound.

The column efficiency was assessed on the basis of apparent stage numbers NTP_i from 'analytical' injections using the well-known approximation[12]

$$NTP_i = L_c \cdot HETP_i \approx 5.54 \frac{t_{R,i}^2}{w_{1/2,i}^2} = 5.54 \frac{(t_{R,i(meas)} - V_{tube}/Q)^2}{w_{1/2,i}^2} \quad (1)$$

where L_c and $HETP_i$ are the column length and the height-equivalent to a theoretical plate, respectively. In eq 1, the measured retention time $t_{R,i(meas)}$ was corrected by the delay due to the dead volume of the system, V_{tube}/Q, where Q is the flow rate. $w_{1/2}$ denotes the peak width at half its height. Table 1 lists the column efficiencies obtained experimentally as a function of the flow rate for the two enantiomers. A significant difference can be observed for the NTP values of the two enantiomers. Due to the observed differences in magnitude of the dispersive effect, the transport-dispersive model[13] was employed for the simulation of the elution profiles of the enantiomers, which are later required for determining the adsorption isotherms (see section 2.1.2). In this model different mass transfer coefficients $k_{m,i}$, were adjusted for the two components, while the axial dispersion coefficient, D_L, was assumed to be equal for both components. The axial dispersion coefficient was calculated from the Chung and Wen correlation[13] as $D_L = 1.21 \times 10^{-6}$ m^2/s. The molecular diffusion coefficient required for these calculations was estimated as $D_m = 3.62 \times 10^{-9}$ m^2/s using the Stokes–Einstein equation.[14] The two mass transfer coefficients $k_{m,1}$, and $k_{m,2}$ were obtained from the measured HETP values by fitting the latter to the following relation:[12]

$$HETP_i(u) = \frac{2D_L}{u} + 2\left(\frac{k'_{0,i}}{1 + k'_{0,i}}\right)^2 \frac{u}{k'_{0,i} k_{m,i}}, \; i = 1,2 \quad (2)$$

where $u = Q/\varepsilon_\tau A$ is the interstitial velocity and $k'_{0,i}$ the retention factor for the respective components. The coefficients obtained were $k_{m,1} = 245.9$ min^{-1} and $k_{m,2} = 58.8$ min^{-1}.

2.1.3. Determination of Adsorption Isotherms. Adsorption isotherms were determined using the inverse method (peak fitting).[13] This corresponds to minimizing the difference between experimentally obtained and simulated elution profiles. For the simulation, the transport-dispersive model was implemented in *Matlab* (Ver. 7.8, MathWorks, U.S.A.) with a spatial discretization of $\Delta z = 2D_L/u$ (ref 15, p 49) and an approximate stability criterion based on the Henry coefficient of the more strongly adsorbed component (ref 15, p 152).

When using the inverse method, it is important to describe the injection profiles accurately.[13] Here we describe both the front (f) and the rear (r) of each injection profile by the following simple approximation:

$$c_i(z = 0, 0 \le t \le t_i) = \frac{c_{max,i}}{1 + \exp \frac{t_i - t}{w_i}}, \; i = (f, r) \quad (3)$$

In the above expression, $c_{max,i}$ (i = f, r) is the maximum height of an injection profile, while t_i and w_i are parameters determined by least-squares fitting eq 3 to the measured front and the rear sections of the injection profiles, determined in the absence of a column.

Two examples of fitted injection profiles are shown in Figure 2 together with a comparison of the model employed here to a more detailed, but numerically too inefficient, continuously stirred-tank-reactor CSTR model of the injection system.

Adsorption was assumed to occur predominately according to the bi-Langmuir mechanism leading to the following isotherm equation:

$$q_i = q_{S1,i} \frac{b_{1,i} c_i}{1 + b_{1,i} c_i} + q_{S2,i} \frac{b_{2,i} c_i}{1 + b_{2,i} c_i} \text{ with } i = 1,2 \quad (4)$$

In order to reduce the number of free parameters to be determined, the Henry constants of both enantiomers were determined using very small injections and were estimated as $H_1 = 0.536$ and $H_2 = 3.808$. These initial slopes of the adsorption isotherms were kept constant in the later calculations by requiring $H_i = q_{S1,i} b_{1,i} + q_{S2,i} b_{2,i}$ ($i = 1, 2$). Furthermore, it was assumed that the first adsorption site is nonselective, i.e. $q_{S1,1} = q_{S1,2}$ and $b_{1,1} = b_{1,2}$, and that the saturation capacity on the second chiral adsorption site is equal for both enantiomers, i.e. $q_{S2,1} = q_{S2,2}$. These assumptions reduce the number of variable parameters to three.

For the parameter determination, a set of six different experiments close to the solubility limit of a racemic mixture, with injection volumes of 200, 1000, and 2400 μL each at two injection concentrations of 10.3 and 20.6 g/L, respectively, were performed. The three free parameters were then determined by simultaneously minimizing the least-squares difference between simulated elution profiles and those recorded in the six experiments. The corresponding results are shown in Figure 3. To confirm the quality of the model parameters derived from the fit, they were validated against independent experimental runs with asymmetric composition as shown in Figure 4. The agreement achieved is considered very good.

The isotherm parameters obtained from the fitting procedure are listed in Table 2. The adsorption isotherms calculated using these parameters are valid up to concentrations of approximately 20 g/L.

2.2. Identification of Operating Parameters for SMB Chromatography. *2.2.1. Theoretical Approach.* As for the determination of the adsorption isotherms, the transport-dispersive model was used to represent the chromatographic separation. Triangle theory,[16] one of the short-cut design methods based on equilibrium theory, was used to identify initial operating parameters for SMB chromatography. The design parameters in triangle theory are defined by the ratio of the net flow-rate of liquid to the simulated

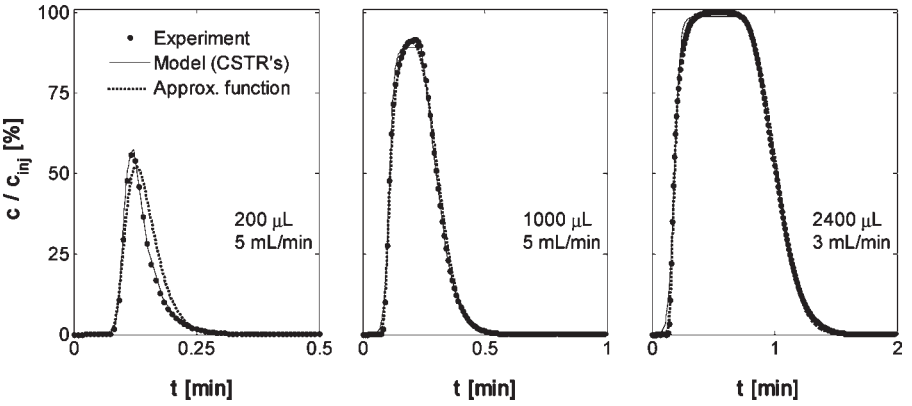

Figure 2. Modeling of injection profiles for the chromatographic runs devoted to quantify the adsorption isotherms. The graphs reveal minor differences between experimental data (dotted) and the two fitted models of a continuously stirred-tank-reactor CSTR (solid line) and the approximation function as described in section 2.1.2.

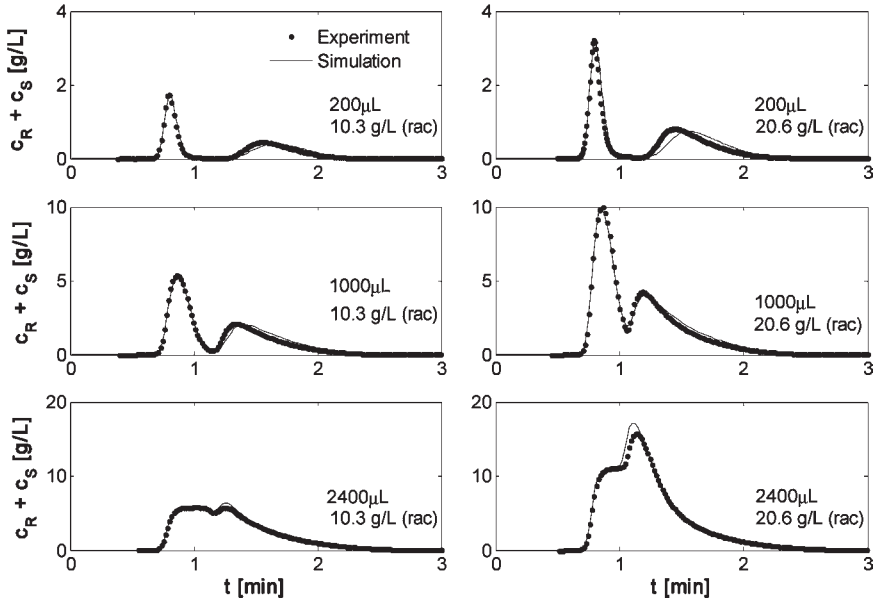

Figure 3. Results of the inverse method applied to six different chromatographic experiments. Comparison of experimental data and fitted elution profiles using a single set of parameters.

flow-rate of solid as shown below,

$$m_i = \frac{Q_i t_S - \varepsilon_T V_C}{(1-\varepsilon_T)V_C} \tag{5}$$

where ε_T is the total porosity of the packed column, Q_i is the volumetric flow-rate of the liquid in zone i, t_S is the port switching interval, and V_C is the volume of the column. Since the SMB process has five fundamental operating parameters (the four flow rates, Q_i, and the switching time, t_S), the process can be designed on the basis of the four expressions for the zone flow-rate ratios m_i above after fixing one parameter. Here, a constraint on the switching time was used (see below). The most promising SMB operating conditions that maximize throughput while delivering the required outlet purities can then be found by optimizing the four zone flow-rate ratios. Each zone flow-rate ratio has to ensure a proper functioning of the corresponding zone.

Four objective functions representing the goal of the corresponding zones can be defined as:

$$G_1 = \log\left(\frac{M_{B,Rc}}{M_{Min,Rc}}\right) \tag{6}$$

$$G_2 = \log\left(\frac{1-Pur_{B,Extr}}{1-Pur_{Target}}\right) \tag{7}$$

$$G_3 = \log\left(\frac{1-Yld_{Target}}{1-Yld_{B,Extr}}\right) \tag{8}$$

$$G_4 = \log\left(\frac{M_{Min,Rc}}{M_{A,Rc}}\right) \tag{9}$$

dx.doi.org/10.1021/op200136z |*Org. Process Res. Dev.* 2012, 16, 331–342

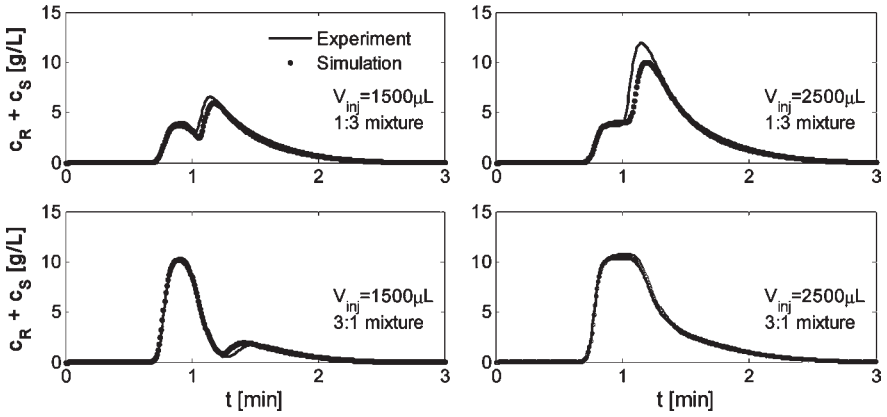

Figure 4. Model validation against independent experiments with asymmetric injection composition. The experiments shown were not used in the inverse method.

Table 2. Estimated adsorption model parameters

parameter		(*R*)-bicalutamide, *i* = **2**	(*S*)-bicalutamide, *i* = **1**
$q_{S1,i}$	[g/L]	43.33	43.33
$b_{1,i}$	[L/g]	0.01026	0.01026
$q_{S2,i}$	[g/L]	15.02	15.02
$b_{2,i}$	[L/g]	0.00609	0.22387

Here, G_j is the objective function, $Pur_{B,Extr}$ and $Yld_{B,Extr}$ are the actual purity and yield of component B (A is the nontarget component) at the extract port, respectively. Pur_{Target} and Yld_{Target} are the target values for purity and yield, respectively. Since the mass flux of solutes are exponentially increased or decreased by the changes of the zone flow-rate ratios, the logarithm values were used to linearize the relationship between the objective values and the flow rate ratios.[17] Note that the objective function G_j corresponds to the zone logarithm error of which sign indicates the direction to increase or decrease corresponding zone flow-rate ratio. $M_{Min,Rc}$ is the minimum mass ratio of each component allowed for recycling between zones 1 and 4 in one port switching interval. Because of the periodic port switching in SMB operation, it is difficult to quantify the recycled amount between zones 1 and 4. We therefore assumed that the liquid-phase concentration profiles in zones 1 and 4 are constant to the average concentrations of zone 1 inlet and zone 4 outlet, respectively. On the basis of these assumptions, $M_{A,Rc}$ and $M_{B,Rc}$ can be calculated from

$$M_{A,Rc} = \frac{\bar{c}_{A,1in} Q_{Extr}}{c_{A,Feed} Q_{Feed}} \tag{10}$$

$$M_{B,Rc} = \frac{\bar{c}_{B,4out} Q_{Raff}}{c_{B,Feed} Q_{Feed}} \tag{11}$$

where $\bar{c}_{A,1in}$ and $\bar{c}_{B,4out}$ are the average concentrations of component A and B at the inlet of zone 1 and the outlet of zone 4, respectively. Four objectives were fulfilled during all simulations of SMB chromatography with the four design parameters (m_1 to m_4) and one fixed set of operating conditions.

As mentioned above, the separation characteristic of each zone mainly depends on its flow-rate ratio, so that each objective can be fulfilled separately. However, if too small an absolute tolerance for the zone flow-rate ratio is used, the iterative optimization routine, which uses only the gradient to obtain the next step direction, fails to converge due to the influence of the other zones. Convergence of the optimization routine was assured by the proportional−differential method, which is part of the proportional−integral−derivative controller (PID) control method[17,18] used. The direction vector, $\vec{D}$, was calculated with the following equations:

Table 3. Parameters used for the optimization of SMB operating conditions and for the simulations

parameters	value
target purity	70−99.9%
target yield	99%
Tolerance	
total mass balance	0.00005
min. recycled amount	0.001
zone flow-rate ratio	0.00005
objective function	0.01
weighting factors (w_P/w_D)	0.5/0.5
numerical method for PDE	FEM with BUDS scheme
no. of nodes	100 per column
integration method	Implicit Euler
tolerance	0.00001

$$\vec{I}_P = \frac{1}{S_P}(G_1, G_2, G_3, G_4)^T,$$
$$S_P = \sqrt{G_1^2 + G_2^2 + G_3^2 + G_4^2} \tag{12}$$

$$\vec{I}_D = \frac{1}{S_D}\left(\frac{\Delta G_1}{\Delta m_1}, \frac{\Delta G_2}{\Delta m_2}, \frac{\Delta G_3}{\Delta m_3}, \frac{\Delta G_4}{\Delta m_4}\right)^T,$$
$$S_D = \sqrt{\left(\frac{\Delta G_1}{\Delta m_1}\right)^2 + \left(\frac{\Delta G_2}{\Delta m_2}\right)^2 + \left(\frac{\Delta G_3}{\Delta m_3}\right)^2 + \left(\frac{\Delta G_4}{\Delta m_4}\right)^2} \tag{13}$$

$$\vec{D} = \frac{S_D}{2}(w_P \vec{I}_P + w_D \vec{I}_D) \tag{14}$$

dx.doi.org/10.1021/op200136z |*Org. Process Res. Dev.* 2012, 16, 331–342

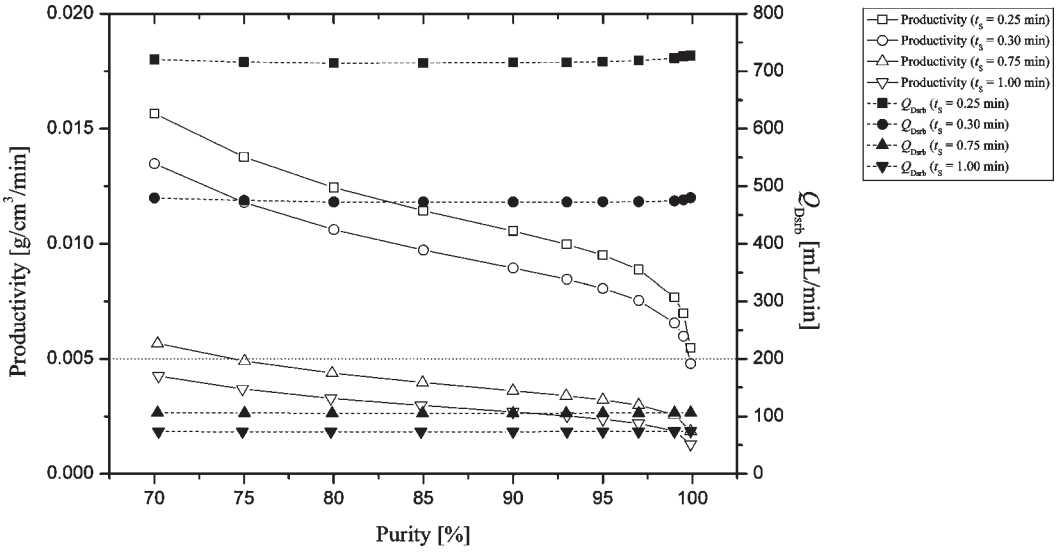

Figure 5. Changes of productivity and desorbent flow-rate as a function of purity of the target component and the port switching interval. Lines are drawn as a guide to the eye.

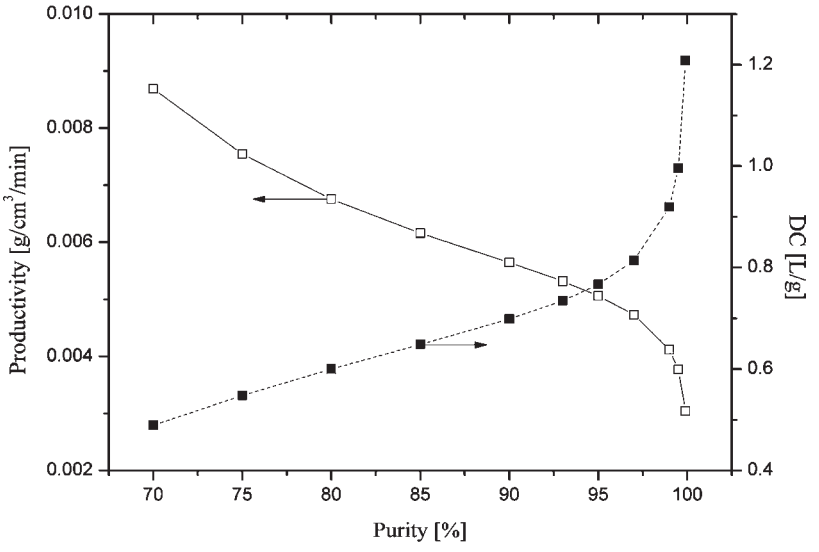

Figure 6. Changes of productivity (open symbols) and desorbent consumption (DC, full symbols) as a function of purity of the target component at the fixed desorbent flow-rate (Q_{Dsrb} = 200 mL/min). Lines are drawn as a guide to the eye.

where $\vec{I}_P$ and $\vec{I}_D$ are, respectively, the unit vectors of the directions calculated from the proportional and derivative gains, w_P and w_D are the weighting factors of the proportional and differential directions ($w_P + w_D = 1$), and S_P and S_D are the vector sizes of the proportional and differential directions, respectively. At the end of the iterations, the proportional and differential vectors for the next iteration were obtained from the previous and current objective functions and zone flow-rate ratio values.

2.2.2. Results of the Estimation Procedure. In order to separate components with high purity and yield, zones 1 and 4 should prevent product streams from being contaminated by the recycled, strongly adsorbed and weakly adsorbed, components, and the minimum mass ratio of recycled component to feed component was limited to 0.1%, ensuring that these conditions are met. Minimization of the loss of target component was achieved by fixing the yield of target component to 99%. The purity of the target component was varied from 70% to 99.9%, surveying the changes of productivity and desorbent consumption. Table 3 summarizes the parameters for the optimization and simulation. The entire SMB simulation was carried out with *Aspen Chromatography*, Ver. 2006.5; Aspen Technology Inc.: Burlington, MA, USA ,and the optimization routine was implemented in Aspen as a Visual Basic script.

The operating conditions were obtained for four zone flow-rate ratios by fixing one set of operating conditions, where the operation constraints determine the exact conditions. The minimum port switching interval was 0.25 min due to the mechanical limitations of the valve system, and the desorbent flow-rate was limited to no more than 200 mL/min in line with the pump capacity. Figure 5 shows the change of both productivity and desorbent flow-rate, Q_{Dsrb}, as a function of target component purity and port switching interval.

Only 0.1% of the total feed amount was allowed to be recycled through zones 1 and 4, so that the concentration profiles in zones

dx.doi.org/10.1021/op200136z |*Org. Process Res. Dev.* 2012, 16, 331–342

1 and 4 are relatively close to zero. This implies that the optimal m_1 and m_4 values are constant to the changes of m_2 and m_3 values, so that the flow-rate at the desorbent port was not changed by the purity of the target component since the desorbent flow-rate is decided by the difference between m_1 and m_4 and the fixed port switching interval ($= (1 - \varepsilon_T)(m_1 - m_4) V_C/t_S$). It increased as the port switching interval shortened. When the port switching interval reached the lower limit, the flow-rate at the desorbent port was over 700 mL/min. The flow rate at the desorbent port was lower than 200 mL/min only when the port switching interval was at least 0.75 min. Consequently, the constraint on the pump flow rate is of greater importance than the port switching interval.

Specific productivities and desorbent consumptions producing the target compound with the required purity and yield were obtained from the optimized operating conditions. Figure 6 shows the changes in productivity and desorbent consumption as a function of the purity of the target component. The port switching intervals were around 0.48 min. In the low purity region (up to 95%), productivity decreases slowly with increasing purity, while the desorbent consumption increases. Once the purity of the target component exceeds 95%, the desorbent consumption increases rapidly with a concurrent rapid decline of productivity. At 99.9% target purity, approximately 60% more desorbent consumption is required compared to a target purity of 95%, and 40% of productivity is lost.

3. COUPLING OF CHIRAL CHROMATOGRAPHY AND SELECTIVE CRYSTALLIZATION

The thermodynamic separation of a pair of enantiomers by crystallization requires comprehensive knowledge of the corresponding solid−liquid phase equilibrium. The eutectic composition is of particular interest, i.e. the composition at the intersection of the solubility isotherm of the single enantiomer and the solubility isotherm of the racemic compound. Kaspereit et al.,[19,20] Gedicke et al.[21] and Amanullah et al.[22,23] proposed a hybrid process coupling SMB chromatography and selective crystallization. The concentration of the target enantiomer delivered by the pre-enrichment step and used as feed for the crystallization step must exceed the eutectic composition. The approach described in the publications cited (denoted 'classical' in the following) is compared to a two-step crystallization process, which was described in a more recent publication,[24−26] together with more detailed solid−liquid phase equilibrium data for bicalutamide in pure methanol and in aqueous solvent mixtures. The process concept is briefly described here, allowing for the derivation of simple mass balances for process quantification.

Solutions of enantiomers of bicalutamide in water or methanol belong to a class of systems that exhibit a shift of the eutectic composition, that can be estimated with a simple shortcut method. Interactions among the heterochiral enantiomers are not pronounced, and solute/solvent interactions prevail. Wang et al.[27] and Klussmann et al.[28] presented two equivalent shortcut methods where the ratio α_r of the solubilities of the stoichiometric compound $x^l_{(R,S)}$ and the single enantiomer $x^l_{(R)}$ (eq 15) is used to express the eutectic composition x^{eu} in solution (eq 16). It is assumed that $x^l_{(R,S)}$ equals the sum of the solubilities of the enantiomers at the stoichiometric (here: racemic) composition of the compound.

$$\alpha_r = \left(\frac{x^l_{(R,S)}}{x^l_{(R)}} \right) \tag{15}$$

$$x^{eu} = \frac{1}{1 + \frac{(\alpha_r)^2}{4}} \tag{16}$$

The Schröder−van Laar equation[29,30] can be used to estimate the ideal solubilities of a compound in solution. The analogous Prigogine−Defay equation[31] allows for the estimation of the ideal solubilities of a racemic compound. Both equations require knowledge of the heat of fusion and the melting point of the solute. Combining both equations with eq 15 leads to an expression for the eutectic composition requiring only the aforementioned calorimetric properties.

$$x^{eu} = \frac{1}{1 + \frac{\left(2 \cdot \sqrt{0.25 \cdot \exp\left[\frac{\Delta h^f_{(R,S)}}{R} \left(\frac{1}{T^f_{(R,S)}} - \frac{1}{T} \right) \right]} \right)^2}{\exp\left[\frac{\Delta h^f_{(R)}}{R} \left(\frac{1}{T^f_{(R)}} - \frac{1}{T} \right) \right]}}{4} \tag{17}$$

Using eq 17, a shift of the eutectic composition of bicalutamide from 98% at 273 K to close to 95% at 333 K is calculated, which correlates well with experimental findings. This shift of the eutectic composition is a prerequisite for the two-step crystallization process adopted here, which is explained in the following. Starting from any asymmetric solution of enantiomers (Figure 7a, point 1, $x^{initial}_{(R)}$), preferential enrichment in the liquid phase can be achieved through solvent removal and subsequent thermodynamic equilibration at low temperature T_{low}. The composition will approach point 2 at the phase boundary between the inner two-phase region and the three-phase region (Figure 7a, shaded), and the solution will separate into a solid phase with racemic composition (point 3) and a liquid phase of eutectic composition (point 4). The eutectic composition $x^{eu,1}_{(R)}$ is richer in the target enantiomer than the initial composition $x^{initial}_{(R)}$ at point 1. This enriched liquid phase is separated from the solid phase and reused at a higher temperature T_{high}. Point 4′ (Figure 7b) represents the initial state for the second crystallization step. There are two options for shifting point 4′ into the outer two-phase region (Figure 7b, shaded), in which selective crystallization of the target enantiomer can take place. Either more solvent is evaporated in order to concentrate the solution up to the phase boundary with the three-phase region, or alternatively, the solubility isotherm can be shifted upwards by controlled addition of an antisolvent. The optimal yield is obtained at the phase boundary between the outer two-phase and the three-phase region (point 4). The solution separates into a liquid phase with the lower eutectic composition $x^{eu,2}_{(R)}$ (point 5) and a solid phase consisting solely of the target enantiomer (point 6).

The change of eutectic composition $\Delta x^{eu}_{(R)} = x^{eu,1}_{(R)} - x^{eu,2}_{(R)}$ with temperature can be relatively large (methionine/water: 8%;[32,33] less for other systems[27,34,35]). The theoretical process yield $Y_{(R)}$, defined as the mass of the pure product over the mass of the excess of the more abundant enantiomer in the initial mixture, depends both upon the difference in the eutectic composition at the respective temperatures and the eutectic composition itself

dx.doi.org/10.1021/op200136z |Org. Process Res. Dev. 2012, 16, 331–342

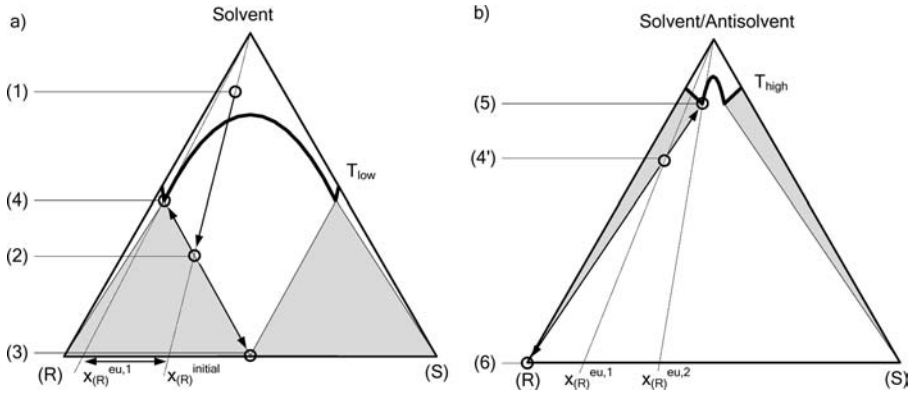

Figure 7. Ternary phase diagram (not to scale) representing the first (a) and the second (b) crystallization step as discussed in the text. (1) liquid phase as obtained from the pre-enrichment step, (2) overall composition after solvent removal, (3) solid- and (4) liquid-phase compositions after equilibration, (4′) overall composition after antisolvent addition, (5) liquid-phase composition after equilibration, (6) product composition.

and can be written as:[24].

$$Y_{(R)} = \frac{1}{(2\cdot x_{(R)}^{\mathrm{eu},1} - 1)} \frac{x_{(R)}^{\mathrm{eu},1} - x_{(R)}^{\mathrm{eu},2}}{(1 - x_{(R)}^{\mathrm{eu},2})} \tag{18}$$

An alternative to eq 18 more suitable for a combined process relates the product mass to the overall amount of the target enantiomer in the fraction, which is obtained from a pre-enrichment step and used as feed for the crystallization process:

$$Y_{(R)}^{\mathrm{tot}} = \frac{(2\cdot x_{(R)}^{\mathrm{initial}} - 1)}{(2\cdot x_{(R)}^{\mathrm{eu},1} - 1)} \frac{x_{(R)}^{\mathrm{eu},1} - x_{(R)}^{\mathrm{eu},2}}{(1 - x_{(R)}^{\mathrm{eu},2})} \tag{19}$$

Analogously, for the classical coupling scheme the theoretical yield can be defined above the eutectic composition[19,20] as:

$$Y_{(R)}^{\mathrm{tot,\,classical}} = \frac{1}{x_{(R)}^{\mathrm{initial}}} \frac{x_{(R)}^{\mathrm{initial}} - x_{(R)}^{\mathrm{eu}}}{1 - x_{(R)}^{\mathrm{eu}}} \tag{20}$$

On this basis, a first estimate of process productivity for the combined processes can be written as:

$$P_{(R)}^{\mathrm{tot,\,classical}} = Y_{(R)}^{\mathrm{tot,\,classical}} \cdot P^{\mathrm{chrom}} \tag{21}$$

$$P_{(R)}^{\mathrm{tot}} = Y_{(R)}^{\mathrm{tot}} \cdot P^{\mathrm{chrom}} \tag{22}$$

The crystallization steps proposed here are entirely defined by thermodynamic states; thus, the fastest crystallization method available can be applied as long as no pronounced mother liquor or impurity inclusion or other kinetically dominated phenomena occur. For this and for practical reasons[24] an antisolvent crystallization was carried out, which approached thermodynamic equilibrium within a few minutes. Apart from crystal purity no further quality criterion was required for the product.

The proposed coupled separation scheme is illustrated in Figure 8. A racemic feed enters unit A (SMB Chromatography) where the extract stream becomes enriched by the target enantiomer and leaves the unit at the port A2. Passing a mixing node, it is concentrated and then further enriched in the first of two crystallization steps (B). Here, a racemic solid fraction is crystallized. The enriched liquid fraction is separated from the solids by filtration and heated to a higher temperature. Water is added as antisolvent, and the product is crystallized and harvested by filtration within step C. The mother liquor remaining after the second crystallization step is of eutectic composition.

Provided that the crystallization equipment is limited in size and that the extract stream emanating from unit A has to be processed batchwise, an internal recirculation of streams is advantageous. More specifically, a fraction of the racemic stream leaving port B4 can be reused and pooled with the stream leaving A2. Furthermore, the eutectic stream leaving C2 can be recycled completely. From the second batch onwards, the same amount of product leaves at port C4 in each subsequent batch, whereas the amount of racemic feed required at port A1 decreases. The overall process yield increases significantly in this manner. The yield involving the decreased outlet stream at port A2 can be balanced as:

$$Y_{(R)}^{\mathrm{recycle}} = 2\cdot x_{(R)}^{\mathrm{initial}} - 1 = \frac{m_{(R)}^{\mathrm{A2,\,reduced}} - m_{(S)}^{\mathrm{A2,\,reduced}}}{m_{(S)}^{\mathrm{A2,\,reduced}} + m_{(R)}^{\mathrm{A2,\,reduced}}} = \frac{m^{\mathrm{C4}}}{m^{\mathrm{A2,\,reduced}}} \tag{23}$$

With eq 23 the productivity of consecutive batches of a coupled process can be calculated as:

$$P_{(R)}^{\mathrm{tot,\,recycle}} = Y_{(R)}^{\mathrm{tot,\,recycle}} \cdot P^{\mathrm{chrom}} \tag{24}$$

4. EXPERIMENTAL SECTION II: PROCESS VALIDATION

4.1. Chemicals and Equipment. The stationary phase used for the adsorption isotherm determination described above was also used for process validation. Four columns with dimensions 10 cm × 2.5 cm (Groupe Novasep SAS, France) were packed with the stationary phase. Pure methanol (>99%, CVM Chemie-Vertrieb Magdeburg GmbH & Co. KG, Schönebeck, Germany) was used as the mobile phase. The columns were installed in a preparative SMB system (CSEP 912 KNAUER SMB production unit, four preparative pumps: K-1800, two UV-detectors: K-2501, Knauer, Germany). The UV detectors operating at 300 nm were used to monitor both the extract and the raffinate port. The SMB unit employed a multifunction valve for connecting up to 12 columns. Operating the SMB unit with fewer columns required a redesign of the tubing, which is explained briefly in the Supporting Information. A comparison of the

dx.doi.org/10.1021/op200136z |Org. Process Res. Dev. 2012, 16, 331–342

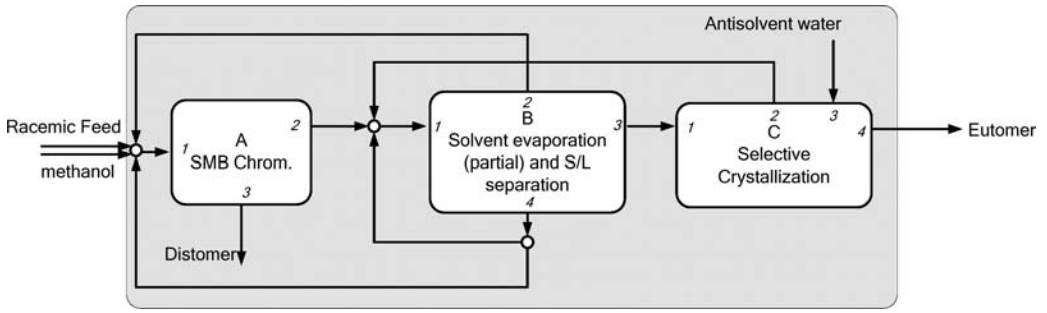

Figure 8. Setup of the proposed coupled process including recycling streams. A racemic feed mixture is pre-enriched by SMB chromatography (A) and further purified in two subsequent crystallization steps (B) and (C). Fractional recycling of the solid phase from (B) and the entire mother liquor from (C) allows for a decrease in the outlet stream A2 and therefore less load onto the chromatographic unit, while keeping the product stream C4 constant.

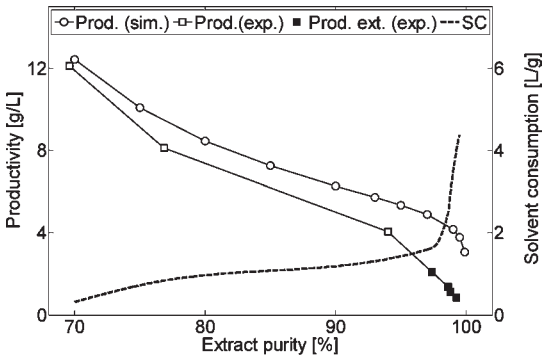

Figure 9. Simulated (open dots) and experimentally determined productivities (squares) for different requirements on the extract purity. Experimental points (open squared symbols) are shifted horizontally to lower purities compared to the corresponding theoretical points (open dots). Full squares denote experimental results after adjusted operation conditions as described in the text. The specific solvent consumption (SC) for the corresponding operation points is also given. Lines are drawn to guide the eye.

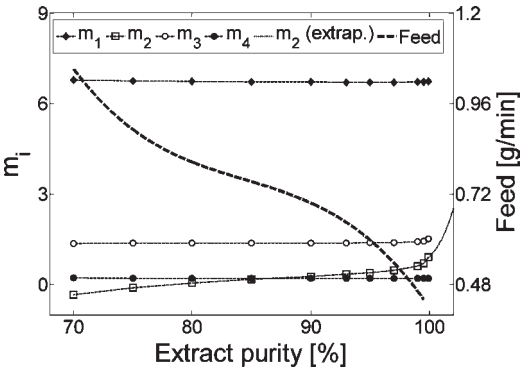

Figure 10. Optimized dimensionless internal flow rate ratios m_i and feed rates for the given extract purities. For the separation task considered, the feed rate correlates to the m_2-value, while all other m_i-values remain constant.

column packing qualities using large injections of bicalutamide revealed very similar elution profiles for all columns. Analogously, the respective porosities of the columns, determined using an unretained solvent, were almost identical, indicating that a good basis for SMB separation existed.

Crystallization was carried out in a 20-L jacketed vessel equipped with a stirrer and a draft tube for agitation, temperature control, and a vacuum pump connected to a reflux cooler suitable for solvent removal. The distillate was weighed automatically using a balance.

The analysis of the product fractions was carried out using a conventional analytical HPLC system consisting of a Dionex P580 gradient pump, an ASI100 automated sample injector, a TCC100 column oven, and an UVD340U DAD detector. The UV-wavelength used for detection was 300 nm. The temperature of the column was controlled at 298 K, and the sample volume injected sample was 5 μL.

4.2. Pre-enrichment by Chromatography. An initial experimental validation of the simulation study was performed for three selected sets of operating parameters. The experimental productivity over purity curve obtained is shown in Figure 9 together with the simulated productivity and the corresponding solvent consumption. Both curves are similar for low extract purities, but deviate increasingly for higher purities. For a given set of parameters, the purity at the extract port was computed as 85%, while the experimental validation revealed an extract purity of 76%. It was found, that in cases, where larger discrepancies between experiment and simulation appeared, zone IV was not capable of entire desorbent regeneration. Thus, traces of bicalutamide entered back into zone I and decreased the purity at the extract port. Clearly, either the adsorption isotherms or the transport coefficients used in the simulation were not chosen optimally or the experimental setup was not sufficiently well represented by the model. Nonetheless, the model was deemed sufficient, since effective pre-enrichment, which is the key property for process coupling, was achieved as shown by Figure 9. Higher extract purities were obtained from a simple extrapolation of the m-values as shown by Figure 10. The plot shows, that all m-values except m_2 are effectively constant for extract purities up to 99.9%. The productivity of the system is therefore governed by the m_2-values and the feed flow rate only. It is generally possible to utilize this information to obtain higher extract purities. The experimentally determined full symbols shown in Figure 9 are based on this rather pragmatic approach. It should be noted that these operating points were optimized for productivity, but that the optimization was performed within a region where the model is less accurate. Thus, more productive operating conditions may exist in addition to those explored here.

The specific solvent consumption per mass of bicalutamide in the extract fraction increases significantly above 98% purity, as can be seen in Figure 9. This is unfavorable, as a purity of 99.5% is required for this compound.

Figure 11 illustrates the productivity as a function of extract purity for a coupled process consisting of a pre-enrichment step based upon the productivity curve determined experimentally and the two-step crystallization process described above.

dx.doi.org/10.1021/op200136z |*Org. Process Res. Dev.* 2012, 16, 331–342

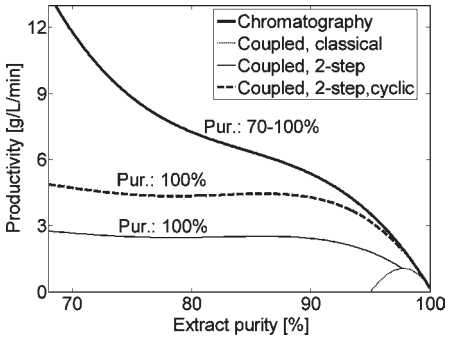

Figure 11. Optimized productivities of the stand-alone chromatographic process (upper thick solid line) and for coupled processes. The classical case (see text) is denoted as a dotted line (lower right corner), while the processes as conducted in this work are illustrated by the thin solid line. The gain in productivity for this process considering internal recycling of streams is reflected by the thick dashed line.

The dashed line corresponds to 100% product purity according to eq 22, the solid line corresponds to the experimentally determined line in Figure 9 (lower line). Clearly, a significant increase in productivity can be achieved with the coupled process, provided the pre-enrichment step is optimized for purities below 90%. Interestingly, there is no global optimum but rather a plateau for lower extract purities. Thus, the optimal solution composition leaving the first and entering the second process unit is not limited by a specific extract purity for this particular separation problem. Taking into account the lower solvent consumption at reduced purity requirements, the curve suggests that operating at 70% purity may be the most promising economically. However, solvent consumption was not an issue here, and the purity was lowered only to the start of the productivity plateau at 90% extract purity. The chromatographic separation of racemic bicalutamide was split into two runs. The process parameters and results of the chromatographic separation are given in Table 4.

4.3. Selective Crystallization Employing a Two-Step Process. The chromatographic extract fraction with a volume of 237 L and rich in the (*R*)-enantiomer was fed to the crystallizer in portions and was concentrated to 8.2 L by vacuum distillation at approximately 200 mbar. The vessel was then cooled to 275 K with the aim of establishing a high eutectic composition of ~98% (*R*)-enantiomer in the liquid phase. However, in contrast to the laboratory-scale experiments, no nucleation occurred within an hour of reaching the final temperature. Thus, a negligible amount of racemic bicalutamide was therefore added as seed crystals. Both a peristaltic pump and a vacuum pump were utilized to withdraw the enriched liquid phase, which was filtered using common HPLC frits. The remaining solid phase was removed, analyzed, and stored. The liquid phase was fed back to the cleaned vessel and heated up to 333 K. A defined amount of water (8.0 kg) was then added. Water acts as an antisolvent, reducing the solubility and forcing the solute to crystallize. After equilibration the solid phase was separated from the mother liquor by vacuum filtration. The crystals were then washed with the mother liquor followed by chilled methanol. The solids were then vacuum-dried. The mother liquor was fed back to the reactor and cooled to 283 K in order to crystallize as much of the remaining bicalutamide as possible. Analysis of the chilled mother liquor showed that the bicalutamide content was below the detection limit.

Table 4. Process conditions for the chromatographic separation runs

internal dimensionless flow rates (m_1, m_2, m_3, m_4)	6.713, 0.665, 1.426, 0.203
External Flow Rates	
eluent	23.7 mL/min
feed	200.0 mL/min
raffinate	36.5 mL/min
extract	179.7 mL/min
Volumes	
eluent	256.0 L
feed	30.3 L
raffinate	47.5 L
extract	233.9 L
purity raffinate	99.54 %
bicalutamide in raffinate	274.0 g
purity extract	92.38 %
bicalutamide in extract	322.0 g
mass lost on column, etc.	7.4 g
overall separation time	21:27 hh:mm
switching time	29 s

5. RESULTS OF THE INDIVIDUAL PROCESS STEPS AND PROCESS COUPLING

The pre-enrichment by SMB chromatography was performed over a period of 22 h and resulted in a purity of 92.38% (*R*)-enantiomer at the extract port, which was slightly above the targeted 90% purity. The raffinate was virtually free of the (*R*)-enantiomer.

The results of the individual crystallization steps are summarized in Figure 12. The values given in brackets denote the theoretical values. Although a broad agreement of the experimental values with the expected values is observed, the deviation of the solid phase (SP) yield and purity from the first crystallization step is significant but can be accounted for. The mother liquor level was well below the upper end of the draft tube after solvent evaporation, which led to poor mixing and pronounced splashing of the liquor onto the reactor internals and the reactor wall. Evaporation of the solvent from these drops resulted in a solid crust with the same enantiomer ratio as the mother liquor. The purity of the solids crystallized from the bulk solution was found to be 56% (*R*)-enantiomer. Since both solid fractions were combined, the resulting total composition was 70% (*R*)-enantiomer, reducing the amount of the target enantiomer in the liquid phase and consequently reducing the yield after the second crystallization step. The optical purity of the product was close to 100%. It is advantageous that the mother liquor in the second crystallization step has a high purity, as this reduces the probability of the crop purity being reduced by adhering mother liquor. Although not investigated here, it is conceivable to force the system into the three-phase region in order to continue preferential growth of the target enantiomer by further decreasing the temperature. The process conditions are rather favorable for running the process in this manner as a large number of crystals is present and the slope of the solubility curve (see[24]) provides further scope for cooling crystallization, providing nucleation of the distomer can be avoided, increasing the yield of the (*R*)-enantiomer.

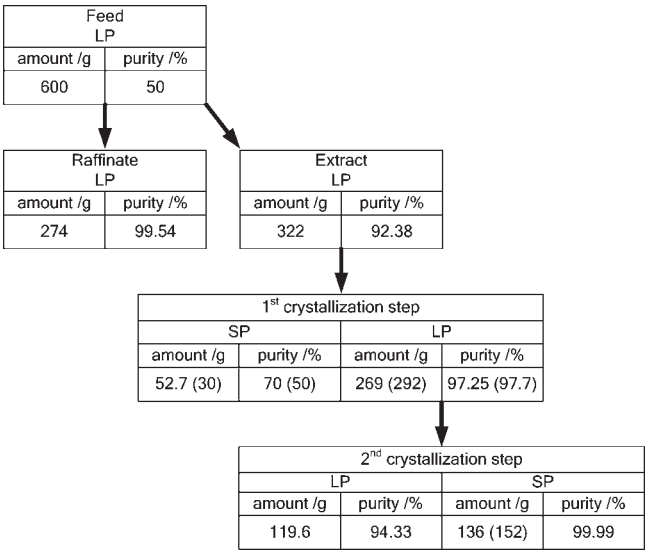

Figure 12. Flowchart illustrating mass balances of the individual purification steps.

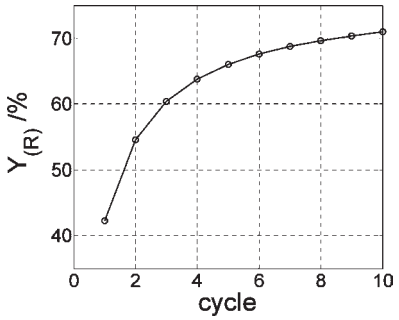

Figure 13. Potential of yield improvements by a series of crystallization batches identical to the one conducted. If experimental stirring issues are avoided and product losses are assumed negligible, complete product recovery would be possible from the second batch on.

The coupling of the two processes presented here rests on a number of assumptions. We are fully aware that a comparison of the coupling of two processes on the basis of a dynamic model for one step and just equilibrium considerations for any following step is always of limited accuracy. Crystallization processes are frequently kinetically dominated, and crystal purities can be correlated with the gradient of the driving force applied. However, this does not apply to the compound considered in this study, and some illustrative numbers may justify this assumption. The accelerated processing of 600 g of racemic bicalutamide developed here requires almost 22 h of chromatographic separation. Generating a product of 99.99% purity using the same equipment requires a considerably longer time due to significantly reduced productivity. Thermodynamic equilibrium was achieved in the first crystallization step within a short period of time after the addition of seeds. The second, antisolvent crystallization was also completed rapidly. Additional time is required for setting up the crystallizer and for product removal and filtration. However, the majority of process steps are either common with the downstream processing of product fractions from a chromatographic unit or can be run parallel to further chromatographic separations. The time required for crystallization and downstream processing becomes negligible, and the chromatographic step is clearly the time-limiting operation in the entire process scheme. However, the behavior of the system investigated here should not be generalized, and other products might require a more detailed investigation.

Figure 11 includes a productivity vs extract purity curve for the classical approach to coupling a pre-enrichment step with selective crystallization (lower right corner, dotted line). Increased productivity can be expected if the pre-enrichment results in a composition that exceeds the eutectic composition, which is >95% in the case of bicalutamide. The range of process conditions where this is achieved is rather narrow for the classical coupling. By using eqs 21 and 22 it can be shown that the productivity of the classical coupling generally outperforms the two-step process for systems with low eutectic compositions (Figure 11, thin solid line). For compounds exhibiting higher eutectic compositions the two-step process is both more efficient and more robust due to the wider range of process conditions available. Furthermore, the two-step process has the potential for a significant increase in the process yield, and exhibits superior productivities compared to the classical coupling for every eutectic composition. When a product is manufactured, generally more than one batch will be made. As discussed above, both the solid phase isolated in the first crystallization step and the mother liquor remaining after the second step can be recycled in subsequent batches, resulting in a considerable improvement in overall yield as shown in Figure 13. Here a series of realistic and imperfect batches identical to the one conducted (losses in the first crystallization step) were considered. Assuming there are no process-dependent losses of material, the second batch already allows 100% of the excess of the more abundant enantiomer in the extract fraction to be harvested (not shown). Higher yields in the crystallization process also lead to a higher productivity of the coupled process, shown as the thick dashed line in Figure 11.

6. SUMMARY AND CONCLUSIONS

The isolation of a single enantiomer from a pre-enriched mixture of bicalutamide enantiomers was successfully scaled up from the laboratory scale[24] using only a few grams of material to a scale of 600 g of racemate. The throughput of the pre-enrichment step employing SMB chromatography was increased at the expense of product purity in this step. The fraction leaving the extract port was subject to two subsequent crystallization steps. Both steps increased the chiral purity, and the final product was 99.99% pure. Experimental issues prevented the theoretical yield of 56% (*R*)-bicalutamide (with respect to the initial amount of (*R*)-bicalutamide in the initial mixture. Thus, the theoretical yield after the first step was reduced to 42%. The determined yield was actually found to be slightly higher (45%), which might be attributed to preferential crystallization during filtration of the crop. When compared to a classical separation scheme (where the enantiomers are separated by chromatography and crystallization) that merely serves to isolate the single enantiomer, it was shown that this type of coupled process is capable of significantly improving the productivity when isolating a single enantiomer from a racemic solution. The productivity and yield can be further enhanced by recycling the waste streams from the first and second crystallization steps in subsequent batches. The approach adopted here is superior to alternative processes for the compound studied and is likely to be beneficial for any system with a eutectic rich in the single enantiomer. The theoretical framework presented can serve as a generic guideline for other chiral separation problems with similar characteristics.

■ ASSOCIATED CONTENT

Supporting Information. This material is available free of charge via the Internet at http://pubs.acs.org.

■ AUTHOR INFORMATION

Corresponding Author

henning.kaemmerer@evonik.com

Present Addresses

[¶]Evonik Industries AG, 63457 Hanau, Germany

[#]Friedrich-Alexander University of Erlangen-Nuremberg, Chair for Separation Science & Technology, 91058 Erlangen, Germany

■ ACKNOWLEDGMENT

This work was part of the European Union FP7 Project 'INTENANT', funded by Grant Number FP7-NMP2-SL2008-214129.[11] The support is gratefully acknowledged. In addition, we thank Dr. Jan von Langermann, Jacqueline Kaufmann, Martin Uxa, and Antje Hofmann for the comprehensive support in the experimental work.

■ NOMENCLATURE

A	column cross-sectional area mm^2
α_r	ratio of the solubilities of the stoichiometric compound and the single enantiomer
$b_{1,i}$	bi-Langmuir model adsorption parameter, site 1, component i L/g
$b_{2,i}$	bi-Langmuir model adsorption parameter, site 2, component i L/g
$\bar{c}_{A,1in}$	average concentration of component A at the inlet of zone 1 g/L
$\bar{c}_{B,4out}$	average concentration of component B at the outlet of zone 4 g/L
c	liquid-phase concentration g/L
$c_{max,f}$	concentration maxima of injection profile g/L
$\vec{D}$	direction vector
D_c	column diameter mm
D_m	molecular diffusion coefficient m^2/s
D_L	axial dispersion coefficient m^2/s
ε_T	total void fraction
G_j	objective function
HETP	height of a theoretical plate mm
i	enantiomers: 1, (S)-bicalutamide; 2, (R)-bicalutamide
$\vec{I}_P,\vec{I}_D$	unit vectors of proportional and differential directions
K	component
$k_{m,i}$	mass transfer coefficient of component i 1/min
k'_0	retention factor
$k_{\Delta p}$	pressure drop coefficient bar s/m
L_c	column length mm
m_j	dimensionless zone flow rates in SMB process
$M_{Min,Rc}$	minimum mass ratio of each component to be recycled between zone 1 to zone 4
$M_{i,Rc}$	mass of component i to be recycled between zone 1 to zone 4
NTP	number of transport plates
$Pur_{i,Extr}$	purity of component i at the extract port
Pur_{Target}	purity of target component at the extract port
p	pressure bar
Q_{Dsrb}	desorbent flow rate mL/min
Q	flow rate mL/min
q_i	solid-phase concentration of component i g/L
$q_{S1,i}$	saturation capacity of component i at the S1 sites at saturation g/L
$q_{S2,i}$	adsorption of component i at the S2 sites at saturation g/L
S_P,S_D	vectors sizes
$t_{R,i}$	retention time of component i min
t_f	retention time of the peak front min
t_r	retention time of the peak tail min
$t_{R,i}$	retention time of component I min
$t_{f/r}$	retention time segregating peak front and peak tail min
t_s	port switching interval in SMB process min
u_0	superficial velocity cm/min
V	column volume mm^3
V_{tube}	volume of tubings, connectors, etc. mL
w_P,w_D	weighting factors
w_f	empirical factor to describe the peak front
w_r	empirical factor to describe the peak tail
$w_{1/2,i}$	width of a peak at half its height of component i min
$x^I_{(R,S)}$	fraction of the racemic compound
$x^I_{(R)}$	fraction of the (R)-enantiomer
x^{eu}	eutectic composition
$Yld_{B,Extr}$	yield of component i at the extract port, respectively
Yld_{Target}	yield of the target component at the extract port
z	axial locus in column mm

■ REFERENCES

(1) Wirth, M. *J. Urol.* **2004**, 172.
(2) Thijs, L. U.S. Pat. Appl. 2003/0073742, 2003.
(3) Tucker, H.; Chesterson, G. J. *J. Med. Chem.* **1988**, *31*, 885.
(4) Zazhi, Z. Y. G. *Chin. J. Pharm.* **2006**, *37*, 73.
(5) Sörös, B. WO 01/00608, 2006.
(6) Ekwuribe, N. N. WO 01/28990, 1999.
(7) James, K. D.; Ekwuribe, N. N. *Tetrahedron* **2002**, *58*, 5905.
(8) *MDL ISIS*, 2.5; Available Chemicals Directory (ACD) commercial catalogue database.
(9) Fujino, A. *Tetrahedron Lett.* **2007**, *48*, 979.
(10) Sugai, T.; Ikunaka, M. JP 2008007492, 2008.
(11) See: www.intenant.eu.
(12) Guiochon, G.; Felinger, A.; Shirazi, D. G.; Katti, A. M. *Fundamentals of Preparative and Nonlinear Chromatography*, 2nd ed.; Academic Press: Boston, 2006.
(13) Chung, S. F.; Wen, C. Y. *AICHhE J.* **1968**, *14*, 857–866.
(14) Einstein, A. *Ann. Phys.* **1905**, *17*, 549–560.
(15) Antos, D. Doctoral Thesis, Oficyna Wydawnicza Politechniki Rzszowskiej, Rzeszôw, Poland, 2003.
(16) Storti, G.; Mazzotti, M.; Morbidelli, M.; Carra, S. *AIChE J.* **1993**, *39*, 471–492.
(17) Lee, J. W.; Wankat, P. C. *J. Chromatogr., A* **2010**, *1217*, 3418–3426.
(18) Tan, K. K.; Wang, G.-G.; Hang, C. C.; Hagglund, T. *Advances in PID Control*. Springer Verlag: London, 1999.
(19) Kaspereit, M., Doctoral Thesis, Otto-von-Guericke-University, Magdeburg, Germany, 2006.
(20) Kaspereit, M.; Gedicke, K.; Zahn, V.; Mahoney, A. W.; Seidel-Morgenstern, A. *J. Chromatogr., A* **2005**, *1092*, 43–54.
(21) Gedicke, K.; Kaspereit, M.; Beckmann, W.; Budde, U.; Lorenz, H.; Seidel-Morgenstern, A. *Chem. Eng. Res. Des.* **2007**, *85*, 928–936.
(22) Amanullah, M.; Abel, S.; Mazzotti, M. *Adsorption* **2005**, *11*, 893–897.
(23) Amanullah, M.; Mazzotti, M. *J. Chromatogr. A* **2006**, *1107*, 36–45.
(24) Kaemmerer, H.; Jones, M. J.; Lorenz, H.; Seidel-Morgenstern, A. *Fluid Phase Equilib.* **2010**, *296*, 192–205.

(25) Lorenz, H.; Kaemmerer, H.; Polenske, D.; Seidel-Morgenstern, A. EP08163733.2, 2008.
(26) Lorenz, H.; Kaemmerer, H.; Polenske, D.; Seidel-Morgenstern, A. WO 2010/025968 A2, 2008.
(27) Wang, Y.; LoBrutto, R.; Wenslow, R. W.; Santos, I. *Org. Process Res. Dev.* **2005**, *9*, 670–676.
(28) Klussmann, M.; White, A. J. R.; Armstrong, A.; Blackmond, D. G. *Angew. Chem., Int. Ed.* **2006**, *45*, 7985–7989.
(29) Mullin, J. W. *Crystallization*; Butterworth-Heinemann: Oxford, 1997.
(30) Tulashie, S. K.; Kaemmerer, H.; Lorenz, H.; Seidel-Morgenstern, A. *J. Chem. Eng. Data* **2010**, *55*, 333–340.
(31) Prigogine, I.; Defay, R. *Chemical Thermodynamics*; Longmann: London, UK, 1973.
(32) Polenske, D.; Lorenz, H. *J. Chem. Eng. Data* **2009**, *54*, 2277–2280.
(33) Kaemmerer, H.; Lorenz, H.; Seidel-Morgenstern, A. *Chem. Ing. Tech.* **2009**, *81*, 1955–1965.
(34) Zhang, Y.; Ray, A.; Rohani, S. *Chem. Eng. Sci.* **2009**, *64*, 192–197.
(35) Worlitschek, J.; Bosco, M.; Huber, M.; Gramlich, V.; Mazzotti, M. *Helv. Chim. Acta* **2004**, *87*, 279–291.